Mechanical Behavior and Dilatation of Particulate-Filled Thermosets in the Rubbery State

U. YILMAZER and R. J. FARRIS, *Polymer Science and Engineering Department, University of Massachusetts, Amherst, Massachusetts 01003*

Synopsis

The stress–strain–dilatational response of glass-bead-filled, amorphous, network polyurethanes was investigated above their glass transition temperature. The mechanical–dilatational behavior was studied as functions of filler content, particle size, crosslink density of the polymer, and the surface treatment of the filler. It was found that the stress–strain properties are strongly affected by separation of the filler from the matrix. Measurements of the vacuole formation and growth processes enabled modeling the stress–strain response as well as understanding the ultimate behavior of the composites. Also, it was found that the dilatational response of the composites can be shifted on a single curve given by the second integral of the Gaussian function.

INTRODUCTION

Mechanical behavior of particulate-filled polymers is influenced by the separation of the filler particles from the matrix.[1–13] Vacuoles form and start to grow when the particles dewet from the polymer during deformation. The processes of vacuole formation and growth lead to lower reinforcement by the filler; the material finally becomes unstable and fails. A measure of the loss of reinforcement, caused by separation of the filler from the matrix, can be obtained by monitoring the volume change of the composite. Combined mechanical–dilatational studies can provide a means of distinguishing the nonlinear effects due to cavitation from other nonlinearities encountered in unfilled polymers.[4]

Mechanical–dilatational investigations on particulate-filled elastomers have mostly been made on highly filled, very lowly crosslinked systems of solid propellant materials.[1–5] Mechanical–dilatational studies have also been made on higher crosslinked systems prepared by vulcanization and peroxides,[6–11] as well as on composites with glassy matrices.[12,13]

The purpose of this study is to investigate the effect of cavitation on the mechanical behavior of particulate-filled elastomers of moderate crosslink density. The crosslink density was well controlled here, and the effect of the crosslink density on the mechanical-dilatational response was explored as a material parameter in addition to filler content, particle size, and the presence of a coupling agent.

MATERIALS

Glass beads having average diameters of 25 μm, 80 μm, and 160 μm were used with no surface treatment and also with an amino functionality silane coupling agent treatment. The matrix material was synthesized by reacting diols and

Journal of Applied Polymer Science Vol 28, 3369–3386 (1983)
 CCC 0021-8995/83/113369-18$02.80

TABLE I
Materials Studied[a]

Crosslink density (g·mol/g matrix)	Vol % of filler					
	0	10	20	30	40	50
System I[b]						
0.5×10^{-3}	√				A,B,C	
1.0×10^{-3}	√	A,A*	A,A*	A,A*	A,A*	A,A*
System II[c]						
0.1×10^{-3}	√		B			
0.2×10^{-3}	√		B			
0.3×10^{-3}	√		B			
0.344×10^{-3}	√		B			

[a] The average diameters of the glass beads are indicated as follows: A = 25 μm, B = 80 μm, C = 160 μm. An asterisk denotes coated particles. Unfilled materials are shown by the symbol √.
[b] System I: Diol of 1050 g/g-mol molecular weight and triol of 425 g/g·mol molecular weight.
[c] System II: Diol of 2000 g/g· mol molecular weight and triol of 4100 g/g mol molecular weight.

triols of polyoxypropylene with TDI. The TDI used in this study was a mixture of 80% 2,4-, 20% 2,6-tolylene diisocyanate. Molecular weights of the diols and the triols used are indicated in Table I, where the materials presented in this study are also shown. The crosslink density was controlled by using stoichiometric amounts of glycols and TDI and varying the diol–triol ratio. The reaction was catalyzed by ferric acetyl acetonate.

The reactions were initiated in a vacuum reaction kettle equipped with a mechanical stirrer. The glycols were dehumidified and degassed under vacuum for 2 h at 100°C prior to transferring to the reaction kettle. Previously dehumidified glass beads and the catalyst were added to the kettle, and the mixture was cooled to room temperature while stirring under vacuum. Then the stoichiometric amount of TDI was added. The reaction mixture was stirred under vacuum for approximately 5–15 min, until the viscosity increase was sufficient to prevent settling of the glass beads. The mixture was cast into an open surface, Teflon-coated, aluminum mold having 1 cm × 1 cm × 25 cm rectangular dimensions. The materials were cured at 45°C for 48 h. The composites were observed under microscope to confirm that the glass beads had not settled. The materials studied here are shown in Table I. All filler fractions discussed in this paper are volume fractions.

EXPERIMENTAL

Differential Scanning Calorimetry (DSC). A Perkin-Elmer DSC-2 was used. The tests were done at a heating rate of 20°C/min. The materials were found to be amorphous with the glass transition temperatures indicated in Figure 1. The glass transition temperatures were determined from the inversion points. In composites having the matrix system II, the glass transition temperature is independent of the crosslink density in the range studied here. The crosslink density of 3.44×10^{-4} (g·mol crosslinks/g matrix) is the maximum crosslink density that can be achieved with this system. In composites having the matrix system I, the glass transition temperature is directly proportional to the crosslink density. The matrices having crosslink densities higher than 1.5×10^{-3} (g·mol

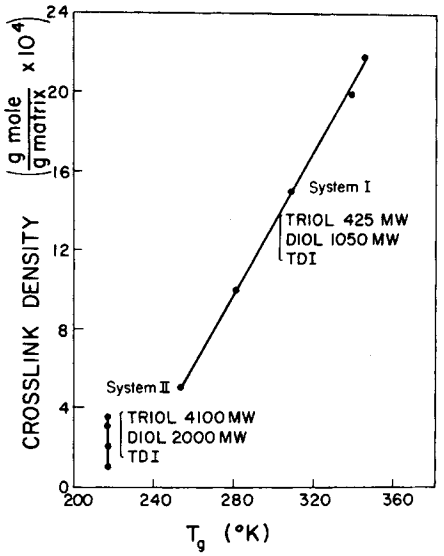

Fig. 1. Crosslink density–glass transition temperature relationship.

crosslinks/g matrix) are glassy at room temperature and are investigated in Ref. 13. The glass transition temperatures were found to be independent of the volume content of the filler, the presence of a coupling agent, and the size of the glass beads in the ranges studied here.

Mechanical–Dilatational Measurements. Mechanical–dilatational measurements were made on rectangular, end-to-end bonded specimens having 1 cm × 1 cm × 7.5 cm (gage) dimensions. The gas dilatometer used in this study operates on the same principle as described in Ref. 13. A photograph of the instrument is shown in Figure 2. An end-to-end bonded specimen, coated for better photographic visibility, is hanging in between the grips of the instrument. The upper grip is connected to the load cell of the dilatometer. The lower grip is connected to the lower crosshead of the Instron. The specimen is in a chamber having a plexiglass door with an *o*-ring seal and swivel locks. The shafts are also sealed by *o*-rings. There is a reference chamber at the back which is not seen. As the specimen extends, the lower shaft moves out of the test chamber and an identical precision-made shaft mounted to the lower shaft enters the test chamber through another bushing and seal. Thus the volume change caused by the extension shaft leaving the test cavity is compensated. The only change of air volume in the test chamber is then due to the change of the volume of the specimen. The change of air volume in the test chamber causes a pressure change which is measured by a fine differential pressure transducer mounted between the test chamber and the constant pressure reference chamber. The pressure changes measured are converted to volume readings by means of calibration. The instrument has a large mass and acts as a heat sink; therefore, the pressure changes due to heating or cooling of the specimen during extension are minimized. This point was confirmed as shown later, since no volume change was observed for the unfilled rubbery matrix material, indicating a Poisson's ratio of 0.5.

The materials were tested at 23°C at a strain rate of 0.266 min^{-1} with the ex-

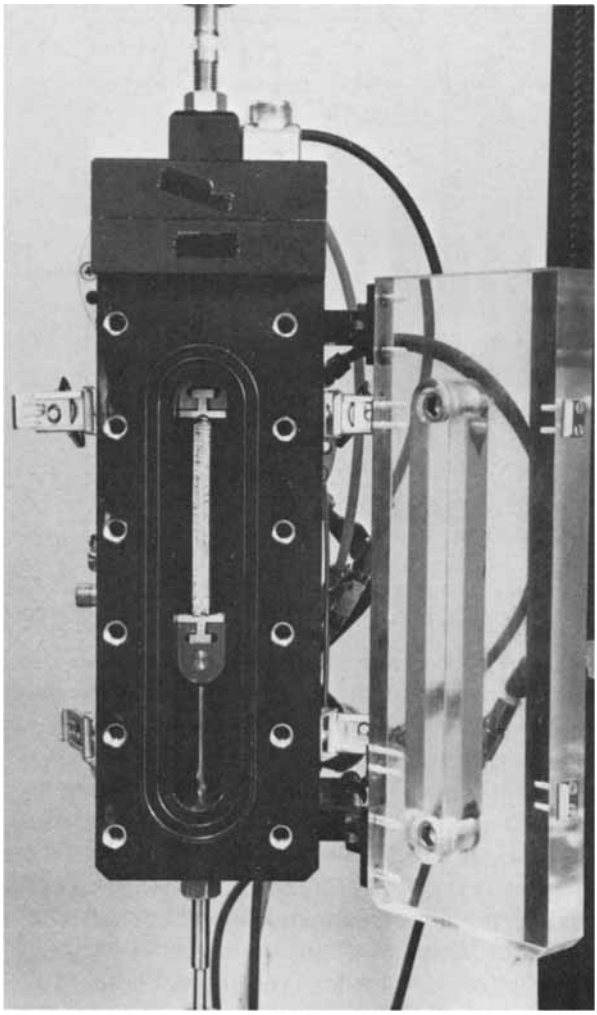

Fig. 2. Photograph of the gas dilatometer.

ception of the materials shown in Figure 16, which were tested at a strain rate of 1.333 min^{-1}.

RESULTS AND DISCUSSION

Effects of Volume Content of the Filler and Coupling Agent on the Mechanical–Dilatational Behavior

Stress–Strain Behavior. Figures 3 and 4 show the stress–strain–dilatational behavior of composites with coated and uncoated particles, respectively. The crosslink density of the matrix is 1×10^{-3} (g·mole crosslinks/g matrix) and the average particle diameter is 25 μm in both figures. The symbols σ, ϵ, V_0 and ΔV are the stress based on the original cross-sectional area, the strain, the original volume of the specimen, and the change in the volume of the specimen, respectively. Filler fractions, ϕ, are indicated on the figures.

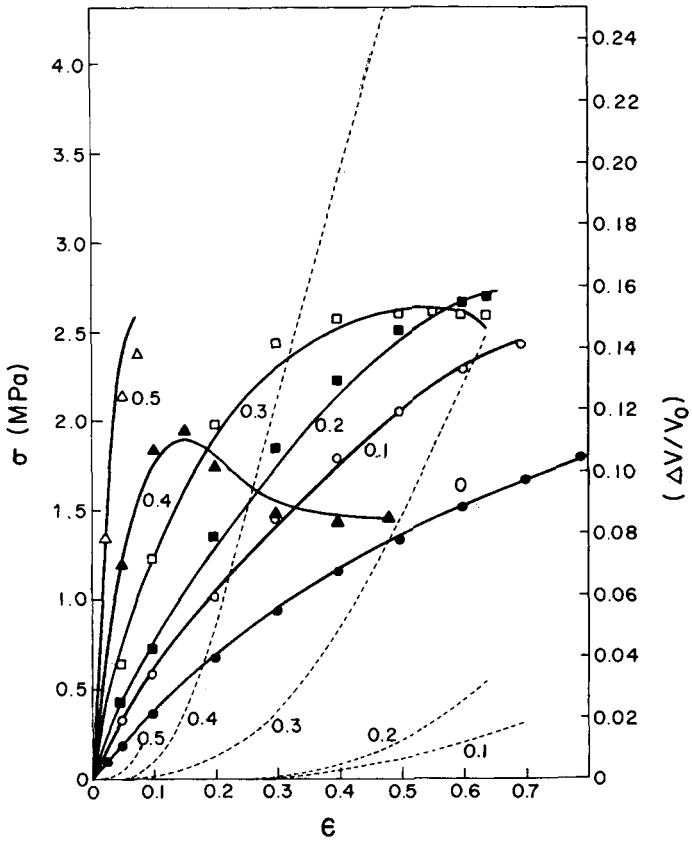

Fig. 3. Engineering stress–strain–dilatational behavior of composites with untreated particles. The points are theoretical values calculated from eq. (4). Exptl: σ (—); $\Delta V/V_0$ (– – –); ϕ: (●) 0; (○) 0.1; (■) 0.2; (□) 0.3; (▲) 0.4; (△) 0.5.

The stress–strain–dilatational behavior can be analyzed in terms of a theory formulated in Ref. 4. The mentioned theory can be summarized as follows: Particles dewet from the matrix and form ellipsoidic vacuoles, the axes of which grow proportionally to the actual strain. Coarser particles dewet earlier in the strain history. There is a distribution in the instantaneous rate of dewetting in a tensile experiment. The instantaneous rate of dewetting is shown to be proportional to $d^2(\Delta V/V_0)/d\epsilon^2$ and the total number of particles that have dewetted is proportional to $d(\Delta V/V_0)/d\epsilon$. The stress is shown to be related to the strain and the dilatation by the following equation.

$$\sigma = E\epsilon \exp[-\beta(\Delta V/V_0)/\epsilon] \tag{1}$$

The theory was tested on highly filled, very lowly crosslinked systems that served as model composites for solid propellant materials. Excellent agreement was obtained in comparisons between the theory and the experiments using β values that varied between 2.65 and 3.66.

Equation (1) states that the nonlinearity in the stress-strain relation is mainly due to vacuole formation and growth. However, the formulation in eq. (1) is valid for highly filled systems in which the vacuole formation process gives rise to the dominating nonlinearity in the stress–strain relation so that the other non-

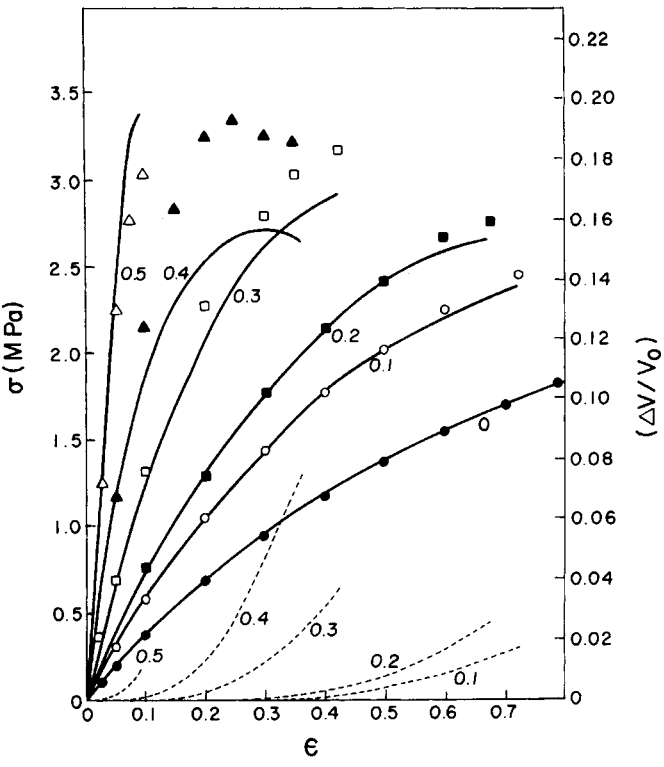

Fig. 4. Engineering stress–strain–dilatational behavior of composites with coupling-agent-treated particles. The points are theoretical values calculated from eq. (4). Exptl: σ (——); $\Delta V/V_0$ (- - -); ϕ: (●) 0; (○) 0.1; (■) 0.2; (□) 0.3; (▲) 0.4; (△) 0.5.

linearities can be neglected. In fact, eq (1) assumes a linear stress–strain relation when the volume change is zero. However, the volume change is very close to zero for unfilled rubbery polymers, but the stress–strain relation is nonlinear. Thus the correct stress–strain relation of the unfilled material must be used to extend the theory to lower filler contents.

There are several choices that give an approximate stress–strain relation for unfilled elastomers. A simple, but effective way, to show the effect of the volume change, is to plot the stress based on the instantaneous cross-sectional area, τ, vs. the strain. Figures 3 and 4 are transformed to true stress vs. ϵ in Figures 5 and 6, by means of the following equation:

$$\tau = \frac{\sigma\lambda}{(V/V_0)} \tag{2}$$

Here V is the instantaneous volume and λ is the extension ratio in the stretch direction.

It is seen that the relation between the true stress and the strain is approximately linear for the unfilled material. Similar observation was made in Reference 14 for other unfilled polyurethane elastomers. However, the stress–strain curves of the filled materials begin to deviate from linearity at the onset of dewetting. This indicates that reinforcement is lost due to dewetting.

Analogous to the stress–strain–dilatation equation of Ref. 4 the following

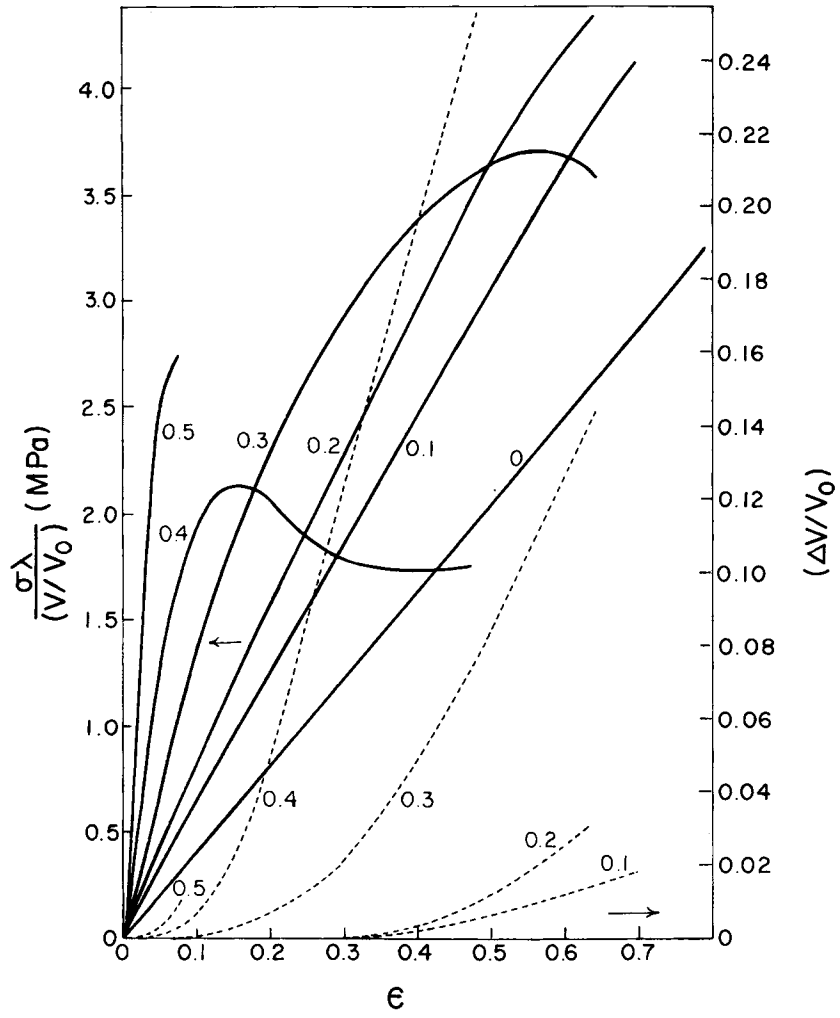

Fig. 5. True stress–strain–dilatational behavior of composites with untreated particles. Volume fractions of the filler are indicated on the figure. Exptl: $\sigma\lambda/(V/V_0)$ (—); $\Delta V/V_0$ (- - -).

equation is proposed between the true stress, strain, and the volume change

$$\tau = E\epsilon \exp[-\beta(\Delta V/V_0)/\epsilon] \tag{3}$$

Combining eqs. (2) and (3), the nominal stress σ is related to the strain and the volume change as follows:

$$\sigma = [(V/V_0)/\lambda]\, E\epsilon \exp[-\beta(\Delta V/V_0)/\epsilon] \tag{4}$$

In Figures 3 and 4 theoretical points calculated from eq. (4) are compared with experimental data. The modulus values used are shown in Table II. The value of β was chosen as 3.7, for all volume fractions in composites with untreated filler as well as treated filler. Small deviations from 3.7 will give a better fit between the theory and the experiments, but the main tenet of the theory is upheld with a constant value of β. In Ref. 4 the relative insensitivity of β was mentioned.

Modulus Reinforcement. The tangent modulus at zero strain, E, is neces-

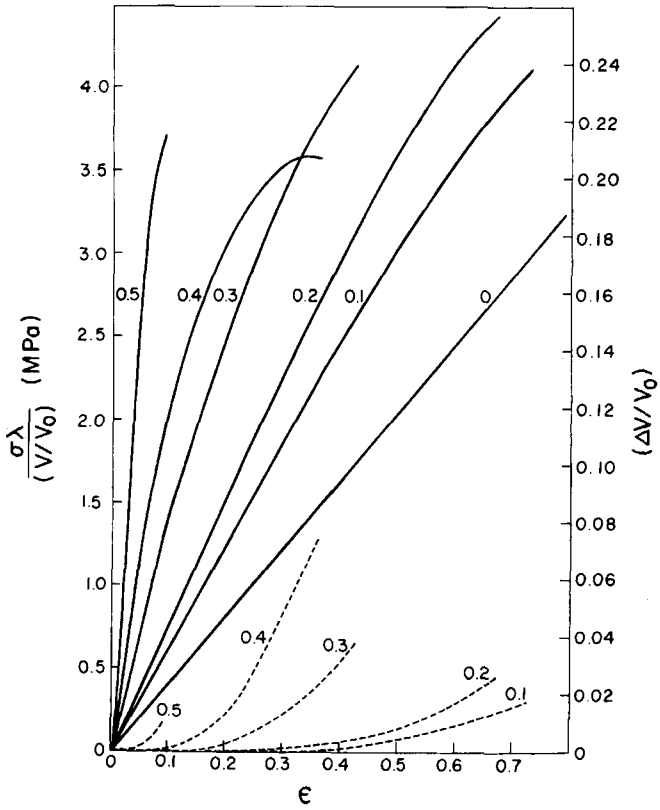

Fig. 6. True stress–strain-dilatational behavior of composites with coupling agent treated particles. Volume fractions of the filler are indicated on the figure. Exptl: $\sigma\lambda/(V/V_0)$ (—); $\Delta V/V_0$ (- - -).

sary in using eqs. (3) and (4). The experimental values of tangent modulus determined from averages on three to five specimens are shown in Figure 7 for the composite systems of Figures 3 and 4. Several equations predicting the relative modulus of the filled systems or the relative viscosity of suspensions were com-

TABLE II
Values of Parameters Used in Calculating the Points in Figures 3, 4, 9, and 10

Filler content	E (MPa)	$\bar{\epsilon}$	s	$V_{f\max}$
	(a) Untreated filler			
0.0	4.20	—	—	—
0.1	6.41	0.475	0.0443	0.080
0.2	8.10	0.460	0.0478	0.176
0.3	13.45	0.305	0.0841	0.430
0.4	25.17	0.130	0.0386	0.714
0.5	55.16	0.060	0.0150	0.570
	(b) Treated filler			
0.0	4.20	—	—	—
0.1	6.20	0.490	0.0342	0.078
0.2	7.65	0.465	0.0421	0.128
0.3	14.13	0.280	0.0473	0.259
0.4	24.13	0.185	0.0346	0.425
0.5	51.02	0.055	0.0097	0.265

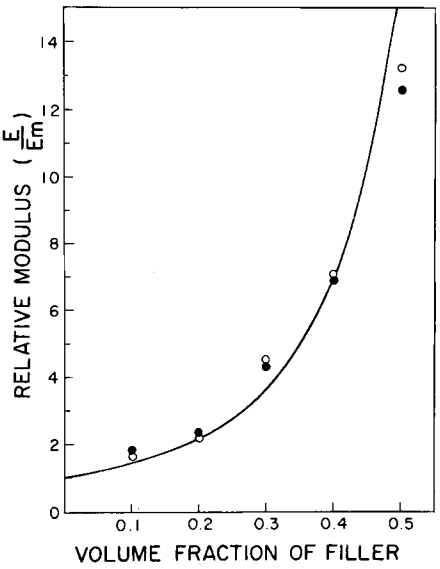

Fig. 7. Relative modulus reinforcement with filler content. (O) Untreated filler; (●) treated filler; (—) theory.

pared with the experimental data. The best agreement was found with an equation proposed for the relative viscosity of suspensions.[15] It is written for relative modulus reinforcement as follows:

$$E/E_m = (1 - \phi/\phi_{\max})^{-2.5} \tag{5}$$

In the above equation, E is the modulus of the composite, E_m is the modulus of the unfilled material, ϕ is the volume fraction of the filler, and $\phi_{\max}$ is the maximum packing fraction of the filler. In using this equation, $\phi_{\max}$ was taken as 0.7405, the value corresponding to hexagonal cubic packing.

The reinforcement in Figure 7 is independent of the presence of the coupling agent. It is concluded later in the paper that the reinforcement is also independent of the crosslink density of the matrix and the particle sizes studied here.

It is pointed out that the reinforcement in the rubbery state is a stronger function of the filler content than it is in the glassy state. In Ref. 13 the reinforcement in the glassy state was found to confirm to Kerner's equation[16] given as in Ref. 17.

Dilatational Behavior. In Ref. 4 the vacuole formation process was modeled and applied to lowly crosslinked, highly filled systems. It was found that the second derivatives of the dilatation–strain curves ($\Delta V/V_0$ vs. ϵ) could be represented by the Gaussian function. A typical dilatation–strain curve represented by the second integral of the Gaussian function is shown in Figure 8. In this figure $\bar{\epsilon}$ is the value of strain about which the Gaussian distribution is centered, s is a measure of the broadness of the distribution, and $V_{f\max}$ is the asymptotic value of $d(\Delta V/V_0)/d\epsilon$ at large strains and is equal to the total volume fraction of solids about which vacuoles are going to form. If all the particles dewet the asymptotic value of $d(\Delta V/V_0)/d\epsilon$ is equal to ϕ. The relations between $\bar{\epsilon}$, s, and

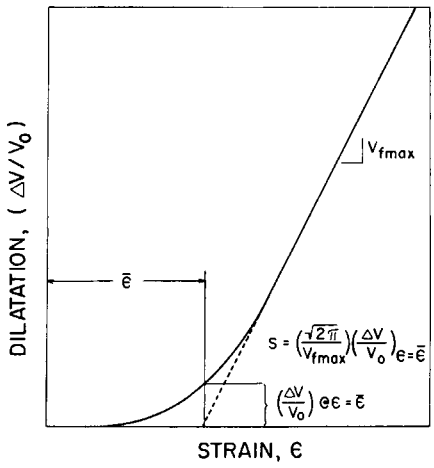

Fig. 8. A schematic representation of a typical dilatation–strain curve given by the second integral of the Gaussian function.

$V_{f\max}$, shown in Figure 8, are the properties of the second integral of the Gaussian function.

In Ref. 4 the dilatation and its first and second derivatives were given by the following equations:

$$\frac{1}{V_0}\frac{d^2\Delta V}{d\epsilon^2} = \frac{dV_f}{d\epsilon} = \frac{V_{f\max}}{s(2\pi)^{1/2}} e^{-n^2/2} \tag{6}$$

where $n = (\epsilon - \bar{\epsilon})/s$

$$\frac{1}{V_0}\frac{d\Delta V}{d\epsilon} = V_f = V_{f\max} \int_{-\infty}^{n} \frac{e^{-n^2/2}}{(2\pi)^{1/2}} dn \tag{7}$$

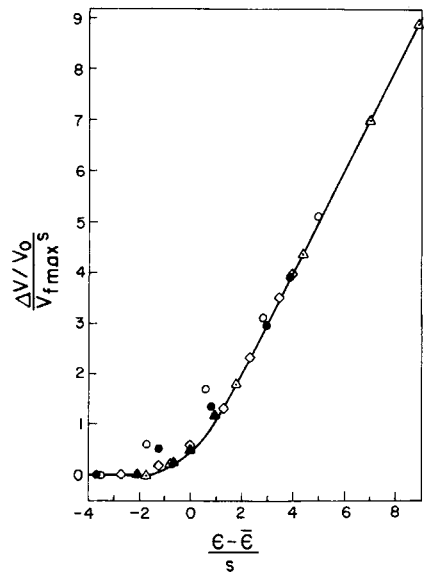

Fig. 9. The dilatation–strain response of composites with untreated filler shifted according to eq. (8). ϕ: (○) 0.1; (●) 0.2; (◇) 0.3; (△) 0.4; (▲) 0.5; (——) Gaussian function.

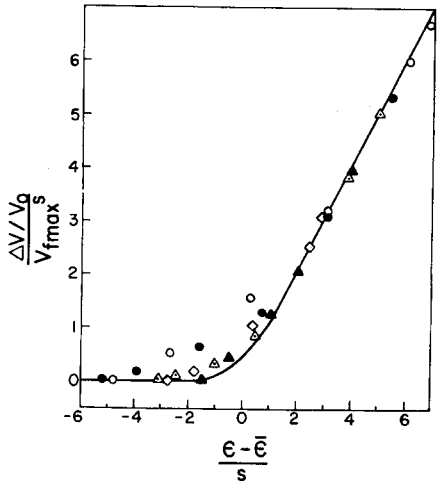

Fig. 10. The dilatation–strain response of composites with treated filler shifted according to eq. (8). ϕ: (○) 0.1; (●) 0.2; (◇) 0.3; (△) 0.4; (▲) 0.5; (——) Gaussian function.

$$\frac{\Delta V}{V_0} = \int V_f d\epsilon = sV_{f\max} \int_{-\infty}^{n} \int_{-\infty}^{n} \frac{e^{-n^2/2}}{(2\pi)^{1/2}} dndn \tag{8}$$

Equation (8) implies that a plot of $(\Delta V/V_0)/(sV_{f\max})$ vs. $(\epsilon - \bar{\epsilon})/s$ should shift the dilatation–strain curves on a single curve which is the second integral of the Gaussian function. Experimental points from the dilatation–strain curves of Figures 3 and 4, shifted in the described manner, are shown in Figures 9 and 10 respectively. The solid line is the second integral of the Gaussian function. The values of $\bar{\epsilon}$, s, and $V_{f\max}$ determined as in Figure 8 are listed in Table II along with moduli values.

The shifted points lie very close to the theoretical line except for the low strain part of the 10% and 20% filled composites. At this strain range and filler content the experimental $\Delta V/V_0$ values are very small; thus the relative errors are amplified. Also at low filler contents the slopes $d(\Delta V/V_0)/d\epsilon$ determined at large strains may not have reached their asymptotic values.

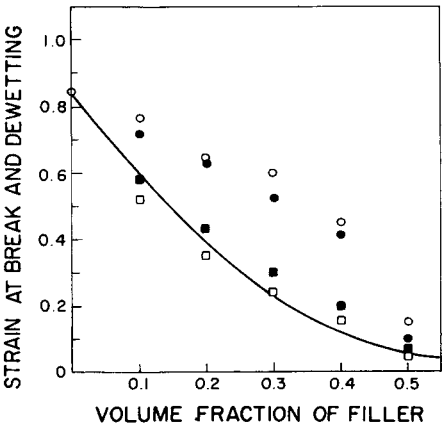

Fig. 11. The strain at break and dewetting as functions of the filler content. The theory is for $\bar{\epsilon}$: (○) ϵ_b untreated; (●) ϵ_b treated; (□) $\bar{\epsilon}$ untreated; (■) $\bar{\epsilon}$ treated; (——) theory.

Ultimate Stress, Strain at Break, and Strain at the Mean Value of Dewetting. The strain at break, ϵ_b, and the strain at the mean value of dewetting, $\bar{\epsilon}$, are shown in Figure 11 as functions of the filler content. The values reported are averages determined from three to five specimens. The strain at the mean value of dewetting, $\bar{\epsilon}$, will be referred as the dewetting strain or the yield strain in the rest of the paper. The dewetting strain is a decreasing function of the filler content. For a given filler content, $\bar{\epsilon}$ is smaller for the untreated filler containing composite than the treated filler containing one. An approximate value of $\bar{\epsilon}$ can be estimated as follows: Assume the adhesion between the matrix and the filler is good, so that adhesive fracture between the filler and the matrix takes place when the elongation of the matrix in between two neighboring particles reaches the extensiblity of the unfilled polymer. The strains encountered by the matrices in between the particles are not homogeneous, but they depend on the initial distance between the neighboring particles among other things. The distribution of the distances between closest particles result in a distribution of strains at which the vacuoles form.

The actual strain in the polymer phase of the composite is greater than the observed strain of the composite, since the extension in the very high modulus glass particles is negligible. The average strain in the polymer phase can be estimated as:

$$\epsilon_{act} = (E/E_m)\epsilon_{obs} \tag{9}$$

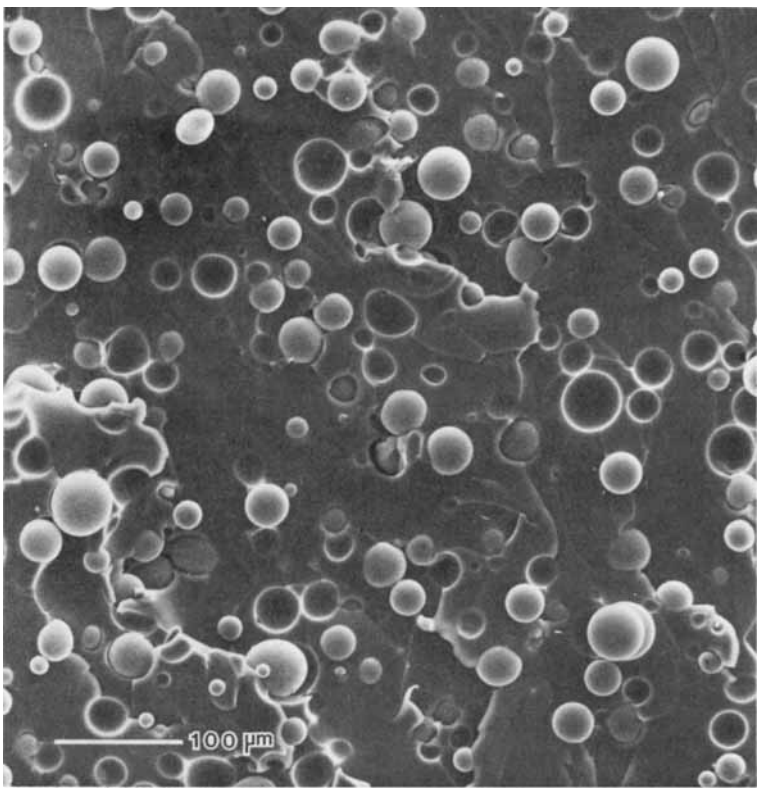

Fig. 12. Scanning electron micrograph (SEM) of the fracture surface of a composite with untreated glass beads.

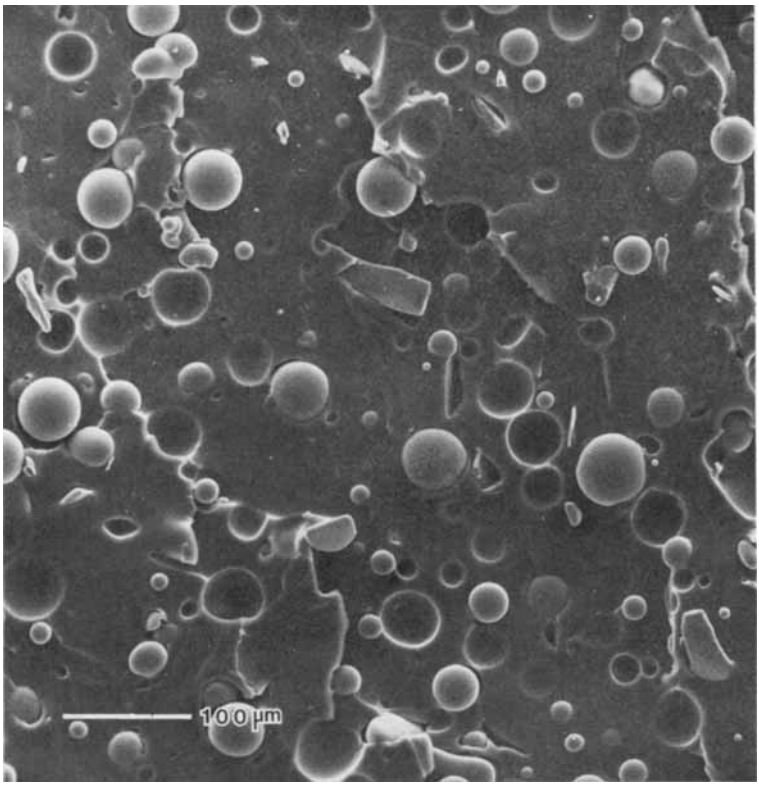

Fig. 13. Scanning electron micrograph (SEM) of the fracture surface of a composite with treated glass beads.

where ϵ_{act} is the actual strain and ϵ_{obs} is the observed strain.

If dewetting takes place when ϵ_{act} reaches a critical value which is close to extensiblity of the unfilled material, ϵ_{cr}, then the observed strain at dewetting is related to ϵ_{cr} by

$$\epsilon_{obs} = \frac{\epsilon_{cr}}{(E/E_m)} \tag{10}$$

The strain $\bar{\epsilon}$ is equal to the average of ϵ_{obs} given in eq. (10). Values of $\bar{\epsilon}$ calculated from eqs. (10) and (5) are compared with experimental data in Figure 11. The degree of adhesion affects the agreement between the theory and the experiments.

The strains at fracture are also shown in Figure 11. The strains at fracture are decreasing functions of the filler content. The untreated filler provides larger strains at fracture since the vacuole formation and growth processes are enhanced in case of untreated filler. This is evident from a comparison of the dilatational behavior. The untreated filler containing composites dewet earlier and reach to higher values of $(\Delta V/V_0)$ before the specimens fracture.

The scanning electron micrographs of the fracture surfaces of the composites containing 20% untreated and treated filler are shown in Figures 12 and 13, respectively. Although the glass beads have clean surfaces in both cases, the treated filler has a smaller fraction of beads that are exposed on the surface.

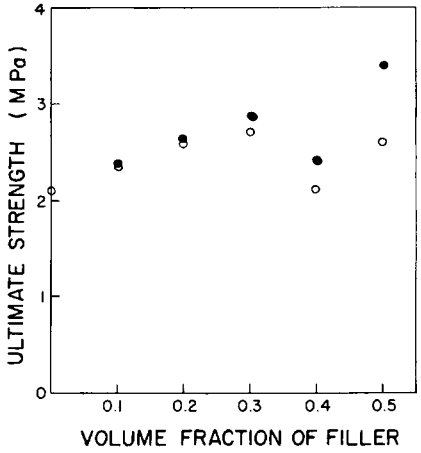

Fig. 14. Ultimate stress of composites as a function of the filler content: (○) untreated filler; (●) treated filler.

Thus the untreated filler provides enhanced vacuole formation and growth leading to higher elongations at break than the treated filler.

The rapid decrease of ϵ_b between 40% and 50% filler content was also observed in composites with a glassy matrix.[13] Fracture takes place without extensive dewetting at high filler contents indicating a change in the mode of fracture.[13]

The ultimate stress of composites are shown in Figure 14. The ultimate stress increases with filler content between 0% and 30% filler loading. A similar observation was made in Ref. 18 in a glass-bead-filled epoxy resin, tested in the rubbery state. However, beyond 30% filler content, it is seen here that the ultimate stress first drops, then increases. The final increase is due to the mentioned change in the mode of fracture from a dewetting one to a relatively nondewetting one. There are two main competing phenomena affecting the ultimate stress. The first one which increases the ultimate stress is the modulus reinforcement. The second one is the loss of reinforcement due to dewetting. There is, of course, the less important viscoelastic relaxation effect. The resultant ultimate stress is determined from the competition of the two main effects. The ultimate stresses of the treated glass-bead-filled composites are greater than that of the untreated glass-filled composites, especially at higher filler contents. These phenomena can be interpreted in terms of the two competing processes that affect reinforcement. The untreated and the treated filler both give the same initial modulus reinforcement. However, the untreated fillers dewet earlier in the strain history, resulting in a higher loss of reinforcement and a lower tensile strength. The effect of early dewetting is stronger at higher filler contents, since there are more particles which can dewet. Thus the observed difference between the tensile strengths of the untreated and treated glass-bead-filled composites is greater at high filler contents.

Effect of Particle Size on the Mechanical–Dilatational Behavior

The stress–strain–dilatational responses of three composites having the same filler content and matrix crosslink density, but different sizes of particles are

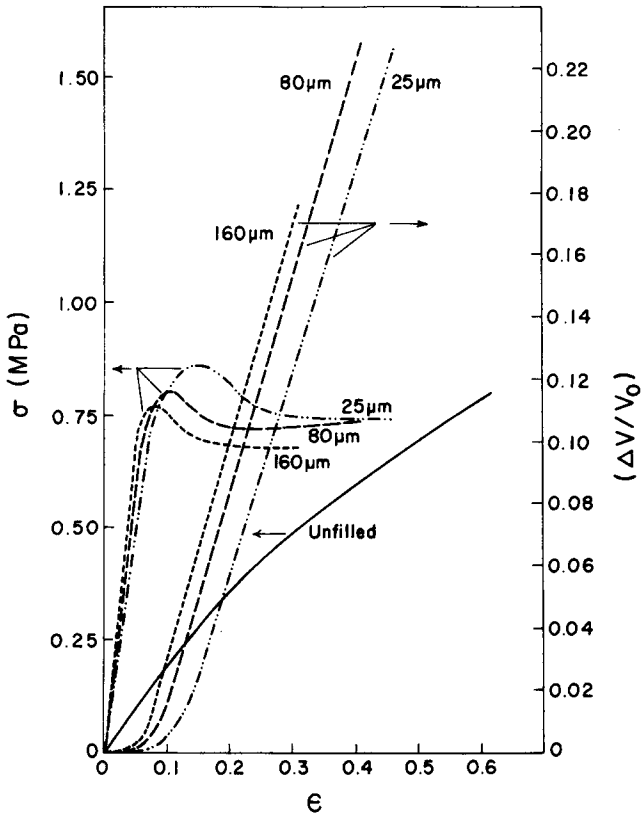

Fig. 15. The stress–strain–dilatational behavior of composites with indicated size of glass beads at 40% filler content.

shown in Figure 15. In this figure the composites have a crosslink density of 0.5 $\times 10^{-3}$ (g·mol/g matrix). The initial modulus is independent of the particle size as observed in other particulate-filled composites.[3,19,20] However, the coarse-particle-filled composites start dewetting at smaller strains; thus the modulus reinforcement is lost earlier and the tensile strength is smaller. The decrease in the ultimate stress with increasing particle size is well known, and theories based on other considerations have been put forward[21,22] to explain this observation. It is also seen that the strain at fracture increases as the particle size decreases. This is not unexpected: The composite with coarser particles start dewetting at smaller strains, and it reaches a critical state of dilatation at smaller strains. At this critical state of dilatation the vacuoles can join in a run-away fashion, giving rise to the failure of the specimen. In fact, the values of dilatation, $\Delta V/V_0$, at fracture of the 25 μm and 50 μm size filled composites are the same, but the dilatation at fracture of the 160 μm size filled composite is less than the others.

An explanation for the earlier dewetting of the coarser particles was given in Ref. 3. It was proposed[3] that, although the stress concentrations are independent of the particle size, the gradient of stress is steeper in smaller particles, thus peak stress concentrations are more rapidly relieved around smaller particles, resulting in less dilatation.

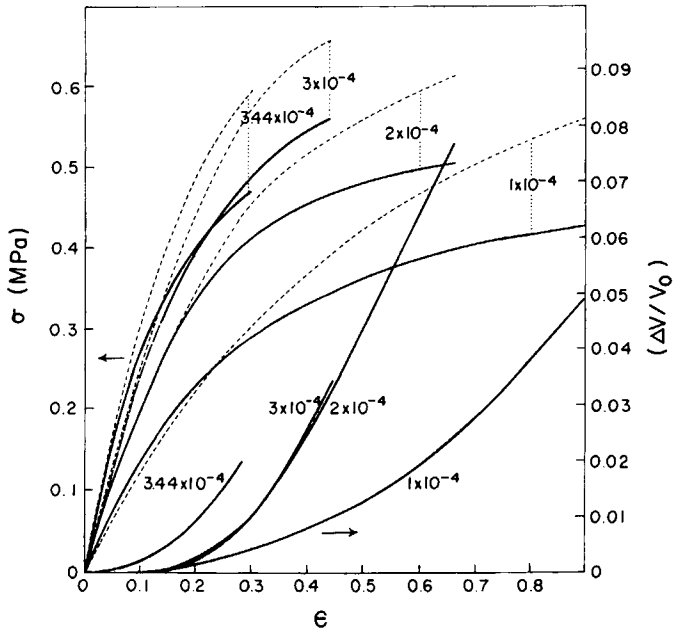

Fig. 16. The stress–strain–dilatational behavior of composites containing 20% untreated filler with an average diameter of 80 μm. The crosslink densities of the matrices in g mol crosslinks/g matrix are indicated on the figure: (—) exptl; (- - -) theory.

The shape of the dilatation–strain curves can be shown to conform to the second integral of the Gaussian function. The asymptotic large strain values of $d(\Delta V/V_0)/d\epsilon$ are the same for the three particle sizes studied here. Calculations have shown that again the stress–strain–dilatation response is of the type given by eq. (4). The value of β is again 3.7 for the 25 μm average diameter particles, but it is somewhat smaller for the other two sizes. It should be noted that the crosslink density of the matrix in Figure 15 is different than it is in Figures 3 and 4. Thus β is approximately independent of the crosslink density of the matrix. The insensitivity of β on the crosslink density is also pointed out later in Figure 16.

Effect of Crosslink Density on the Mechanical–Dilatational Behavior

The stress–strain–dilatational response of composites having the same size and volume content of filler, but different crosslink density of the matrix, is shown in Figure 16. The matrices in this figure are shown as system II in Table II. Two other crosslink densities synthesized from system I glycols were shown in Figures 3 and 15.

Calculations have shown that the relative reinforcement (E/E_m) of the composites are independent of the crosslink density of the matrix. However, the dewetting strain $\bar{\epsilon}$ is a decreasing function of the crosslink density in general. The decrease in $\bar{\epsilon}$ is believed to result from the reduced extensibility of the matrix with increasing crosslink density. The stress value $\bar{\sigma}$, corresponding to $\bar{\epsilon}$, can be found from the intersection of the vertical line drawn from $\bar{\epsilon}$ and the stress–strain curve. The values of $\bar{\sigma}$, shown in Table III, are relatively independent

TABLE III
Stress at the Mean of Dewetting as a Function of the Crosslink Density of the Matrix

Crosslink density (g-mol/g matrix)	$\bar{\sigma}$ (MPa)
1×10^{-4}	0.359
2×10^{-4}	0.403
3×10^{-4}	0.486
3.44×10^{-4}	0.359

of the crosslink density, indicating that the average adhesive strength between the filler and the matrix does not depend on the crosslink density in this system.

The stress–strain–dilatational responses calculated from eq. (4) with a β value of 3.7 are also plotted in Figure 16. The agreement is less satisfactory here due to larger particle size and higher extensibility of the matrix.

With the exception of the lowest crosslinked material, the dilatational curves have the same asymptotic large strain value of $d(\Delta V/V_0)/d\epsilon$, which is equal to the filler fraction of the composite. The shapes of the dilatational curves can again be described by the second integral of the Gaussian function.

CONCLUSIONS

The stress–strain properties of the glass-bead-filled elastomers are strongly affected by dewetting and vacuole growth. The true stress–strain relationship is linear for the unfilled polymer, which does not undergo significant volume change. It is also linear in composites before dewetting takes place. The reinforcement is lost when the matrix is separated from the fillers, and the true stress values are less than linear in this case. The stress–strain relation of the composites can be predicted if the dilatation is accounted for.

The relative modulus reinforcement does not depend on the presence of a coupling agent, the particle size, and the crosslink density of the matrix, but it only depends on the filler content of the composite. The modulus reinforcement is greater in composites with a rubbery matrix than it is in composites with a glassy matrix. The relative modulus reinforcement in the rubbery state can be described by an equation proposed in Ref. 15.

The dilatational response of the composites can be shifted on a single curve given by the second integral of the Gaussian function.

The dewetting strain decreases with increasing filler content, increasing crosslink density and increasing particle size. The dependence of the dewetting strain on the filler content can be predicted with the assumptions put forward in the paper. The dewetting strain is smaller, but the failure strain is larger in untreated glass-filled composites than it is in treated glass-filled composites. The strain at break decreases with increasing filler content, increasing particle size and increasing crosslink density. The ultimate stress increases with filler content between 0% and 30% filler loading. It decreases near 40% filler content, but again increases at higher filler loadings due to the change in the mode of failure. The ultimate stress of the treated glass-bead-filled composites is greater than that of untreated glass-bead-filled composites, since the loss of reinforce-

ment is less for the coupling-agent-treated filler. The ultimate stress also decreases with increasing particle size, since dewetting takes place at smaller strains for larger particles.

This research was supported by the Center for University of Massachusetts—Industry Research in Polymers.

References

1. R. J. Farris, *J. Appl. Polym. Sci.*, **8,** 25 (1964).
2. A. E. Oberth and R. S. Bruner, *Trans. Soc. Rheol.*, **9,** 165 (1965).
3. A. E. Oberth, *Rubber Chem. Tech.*, **40,** 1337 (1967).
4. R. J. Farris, *Trans. Soc. Rheol.*, **12,** 315 (1968).
5. R. F. Fedors and R. F. Landel, *J. Polym. Sci., Polym. Phys. Ed.*, **13,** 579 (1975).
6. H. F. Schippel, *Ind. Eng. Chem.*, **12,** 33 (1920).
7. H. C. Jones and H. A. Yiengst, *Ind. Eng. Chem.*, **32,** 1354 (1940).
8. K. C. Bryant and D. C. Bisset, *Rubber Chem. Tech.*, **30,** 610 (1957).
9. T. L. Smith, *Trans. Soc. Rheol.*, **3,** 113 (1959).
10. R. Shuttleworth, *Eur. Polym. J.*, **4,** 31 (1968).
11. T. Shimamura and M. Takahashi, *Rubber Chem. Tech.*, **43,** 1025 (1970).
12. J. C. Smith, G. A. Kermish, and C. A. Fenstermaker, *Recent Advances in Adhesion*, Gordon and Breach, London, 1973, p. 333.
13. U. Yilmazer and R. J. Farris, *Polym. Compos.*, **4,** 1 (1983).
14. W. Dzierza, *J. Appl. Polym. Sci.*, **22,** 1331 (1978).
15. R. F. Landel, B. G. Moser, and A. J. Bauman, *Proceedings of the Fourth International Congress on Rheology* E. H. Lee, Ed., Wiley-Interscience, New York, 1965, Part 2, p. 663.
16. E. H. Kerner, *Proc. Phys. Soc. B*, **69,** 808 (1956).
17. J. C. Halpin and J. L. Kardos, *Polym. Eng. Sci.*, **16,** 344 (1976).
18. C. Migliaresi, L. Nicolais, L. Nicodemo, and A. T. DiBenedetto, *Polym. Compos.*, **2,** 29 (1981).
19. L. Cohan, *Rubber Chem. Tech.*, **23,** 635 (1950).
20. A. R. Payne, in *Composite Materials*, L. Holliday, Ed., Elsevier, New York, 1966, p. 300.
21. G. Landon, G. Lewis, and G. F. Boden, *J. Mater. Sci.*, **12,** 1605 (1977).
22. H. Alter, *J. Polym. Sci.*, **9,** 1525 (1966).

Received February 15, 1983
Accepted April 18, 1983